Mon. Not. R. Astron. Soc. **000**, 000–000 (0000) Printed 19 June 2002 (MN LaTeX style file v1.4)

Large Scale Structure in the SDSS Galaxy Survey

A. Doroshkevich[1,2] D.L. Tucker[3] & S. Allam[3,4]

1 *Theoretical Astrophysics Center, Juliane Maries Vej 30, DK-2100 Copenhagen Ø, Denmark*
2 *Keldysh Institute of Applied Mathematics, Russian Academy of Sciences, 125047 Moscow, Russia*
3 *Fermi National Accelerator Laboratory, MS 127, P.O. Box 500, Batavia, IL 60510 USA*
4 *National Research Institute for Astronomy & Geophysics, Helwan Observatory, Cairo, Egypt*

arXiv:astro-ph/0206301 v1 18 Jun 2002

19 June 2002

ABSTRACT

The Large Scale Structure (LSS) in the galaxy distribution is investigated using the Sloan Digital Sky Survey Early Data Release (SDSS EDR). Using the Minimal Spanning Tree technique we have extracted sets of filaments, of wall-like structures, of galaxy groups, and of rich clusters from this unique sample. The physical properties of these structures were then measured and compared with the expectations from Zel'dovich' theory.

The measured characteristics of galaxy walls were found to be consistent with those for a spatially flat ΛCDM cosmological model with $\Omega_m \approx 0.3$ and $\Omega_\Lambda \approx 0.7$, and for Gaussian initial perturbations with a Harrison – Zel'dovich power spectrum. Furthermore, we found that the mass functions of groups and of unrelaxed structure elements generally fit well with the expectations from Zel'dovich' theory, although there was some discrepancy for lower mass groups which may be due to incompleteness in the selected sample of groups. We also note that both groups and rich clusters tend to prefer the environments of walls, which tend to be of higher density, rather than the environments of filaments, which tend to be of lower density.

Finally, we note evidence of systematic differences in the properties of the LSS between the Northern Galactic Cap stripe and the Southern Galactic Cap stripe – in particular, in the physical properties of the walls, their spatial distribution, and the relative numbers of clusters embedded in walls. Because the mean separation of walls is $\approx 60 - 70h^{-1}$ Mpc, each stripe only intersects a few tens of walls. Thus, small number statistics and cosmic variance are the likely drivers of these systematic differences.

Key words: cosmology: large-scale structure of the Universe: general — surveys.

1 INTRODUCTION

With the advent of the Durham/UKST Galaxy Redshift Survey (DURS, Ratcliffe et al. 1996) and the Las Campanas Redshift Survey (LCRS, Shectman et al. 1996), the galaxy distribution on scales up to $\sim$300 h^{-1} Mpc could be studied. Now these investigations can be extended using the public data sets from the Sloan Digital Sky Survey Early Data Release (SDSS EDR; Stoughton et al. 2002), which contains $\approx$ 30 000 galaxies in two slices for distances $D \leq 600h^{-1}$Mpc.

The analysis of the spatial galaxy distribution in the DURS and the LCRS has revealed that the Large Scale Structure (LSS) is composed of walls and filaments, that galaxies are divided roughly equally into each of these two populations (with few or no truly isolated galaxies), and that richer walls are linked to the joint random network of the cosmic web by systems of filaments (Doroshkevich et al. 2000; 2001). Furthermore, these findings are consistent with results obtained for simulations dark matter (DM) distributions (see, e.g., Cole et al. 1998; Jenkins et al. 1998) and for mock galaxy catalogues based upon DM simulations (Cole et al. 1998).

The quantitative statistical description of the LSS is in itself an important problem. Beyond that, though, the analysis of rich catalogues can also provide estimates for certain cosmological parameters and for the characteristics of the initial power spectrum of perturbations. To do so, some theoretical models of structure formation can be used.

The close connection between the LSS and Zel'dovich' pancakes has been discussed by Thompson & Gregory (1978) and by Oort (1983). Now this connection is verified by the comparison of the statistical characteristics of observed and simulated walls with theoretical expectations (Demiański & Doroshkevich 1999; 2002, hereafter DD99 & DD02) based on the Zel'dovich theory of nonlinear gravitational instabil-

© 0000 RAS

ity (Zel'dovich 1970; Shandarin & Zel'dovich 1989). This approach connects the characteristics of the LSS with the main parameters of the underlying cosmological scenario and the initial power spectrum, and it permits the estimation of some of these parameters using the measured properties of walls. It was examined with the simulated DM distribution (DD99; Demiański et al. 2000), and was found that, for sufficiently representative samples of walls, a precision of better than 20% can be reached.

Effective methods of the statistical description of the LSS were developed by Demiański et al. (2000) and Doroshkevich et al. (2000; 2001), who applied them to DM simulations and to the DURS and the LCRS. In this paper we apply the same approach to the SDSS EDR, a sample from which we can obtain more representative and more precise measures of the properties of the LSS and the initial power spectrum of perturbations.

We widely use the Minimal Spanning Tree technique. With this technique, we can quantitatively describe the sample under investigation, divide the sample into physically motivated subsamples, and extract different sets of the LSS elements. This technique allows us to discriminate between filamentary and wall–like structure elements located presumably within low and high density regions and to estimate their parameters for the different threshold overdensities bounding them. The same technique allows us to extract sets of groups and rich clusters of galaxies and to measure some of their properties.

Comparison of the observed characteristics of walls with the theoretical expectations (DD99; DD02) demonstrates that the observed galaxy distribution is consistent with Gaussianity initial perturbations and that the walls are the recently formed, partly relaxed Zel'dovich'pancakes. The mean basic characteristics of the walls are consistent with those theoretically expected for the initial power spectrum measured by the CMB observations.

In this paper we also analyse the mass functions of structure elements selected for a variety of boundary threshold overdensities. We show that these functions are quite similar to the expectations of the Zel'dovich' theory, which generalizes the Press – Shechter formalism for any structure elements. In addition, the theory indicates that the interaction of large and small scale perturbations can be important for the formation of the observed LSS mass functions. Our analysis demonstrates that this interaction is actually seen in the influence of environment on the characteristics of groups of galaxies.

This paper is organized as follows: In Secs. 2 we describe the sample of galaxies which we extracted from the SDSS EDR and the method we have employed to correct for radial selection effects. In Sec. 3 we establish the general characteristics of the LSS. More detailed descriptions of filamentary network and walls can be found in Secs. 4 and 5, respectively. In Secs. 6 and 7 we discusse the probable selected clusters of galaxies and the mass function of structure elements. We conclude with Sec. 8 where a summary and a short discussion of main results are presented.

2 THE SDSS EARLY DATA RELEASE

We use as our observational sample the SDSS EDR (Stoughton et al. 2002), which is the first public release of data from the SDSS (Fukugita et al. 1996, Gunn et al. 1998, and York et al. 2000).

The imaging data for the SDSS EDR encompasses 462 sq deg of sky – a $2.5^\circ \times 90^\circ$ equatorial slice in the North Galactic Cap (Runs 752 & 756), a $2.5^\circ \times 66^\circ$ equatorial slice in the South Galactic Cap (Runs 94 & 125), and about 68 sq deg in the direction of the SIRTF First Look Survey (Runs 1336, 1339, 1356, & 1359). The EDR also contains followup spectra, which are available for all but two 2.5×2.5 fields in the North Galactic Cap slice.

We obtained our SDSS EDR sample via the SDSS Query Tool (`sdssQT`)*, a standalone interface to the SDSS Catalog Archive Server. The exact query used in documented in the Appendix.

In our analysis here, we ignore the SIRTF fields and consider just the two equatorial slices. In particular, we consider four samples based upon these two slices:

- N-600, the northern sample for $D \leq 600h^{-1}$Mpc (16 883 galaxies)
- S-600, the southern sample for $D \leq 600h^{-1}$Mpc (12 428 galaxies)
- N-380, the northern sample for $D \leq 380h^{-1}$Mpc (13 698 galaxies)
- S-380, the southern sample for $D \leq 380h^{-1}$Mpc (9 924 galaxies)

2.1 Correction for the radial selection effects

In Figure 1 we plot the radial distributions of galaxies in the N-600 and S-600 samples. Note that the radial selection effects clearly seen in these two distributions are quite successfully fit by curves describing a selection function of the form

$$f_{gal}(D) \propto D^2 \exp[-(D/R_{sel})^{3/2}], \quad R_{sel} \approx 190h^{-1}\mathrm{Mpc}\,, \quad (1)$$

where D is a galaxy's radial distance and R_{sel} is the selection scale (Baugh & Efstathiou 1993).

In some applications, like when we want to correct a measure of the observed density to a measure of the true density, we would like to use equation (1) to correct for the radial selection effects after the fact. An example of such a case is calculating a group's or cluster's true richness based upon the observed number of galaxies it contains (Sec. 6 & 7).

In other applications, however, like in searching for groups or clusters in a magnitude-limited sample, we want to make a preemptive correction for the radial selection effects. For example, in a standard friends-of-friends percolation algorithm (e.g., Huchra & Geller 1982), this is done by adjusting the linking length as a function of radial distance. Here, instead, we employ the rather novel approach of adjusting the radial distances themselves; so, instead of the measured radial distance, we use a modified radial distance, D_{md}, where

$$D_{md}^3 = 2R_{sel}^3(1 - [1 + (D/R_{sel})^{3/2}] \exp[-(D/R_{sel})^{3/2}])\,. \quad (2)$$

* http://archive.stsci.edu/sdss/software/#sdssQT

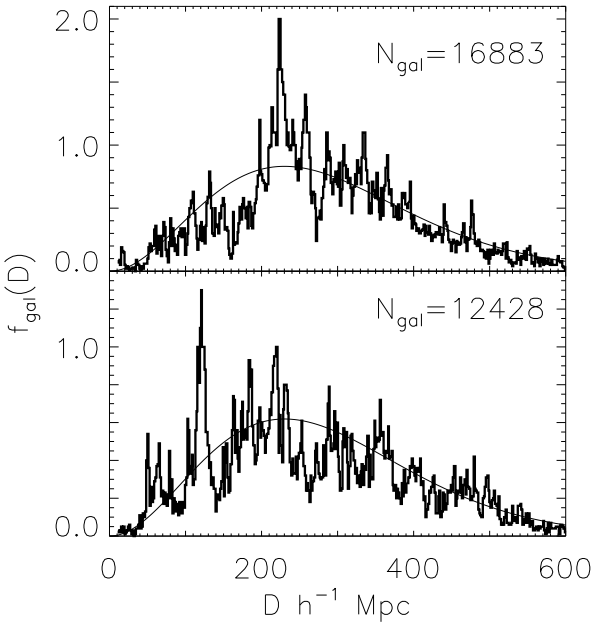

Figure 1. The radial galaxies distributions in the samples N-600 (top panel) and S-600 (bottom panel). The selection function (1) is plotted by solid lines.

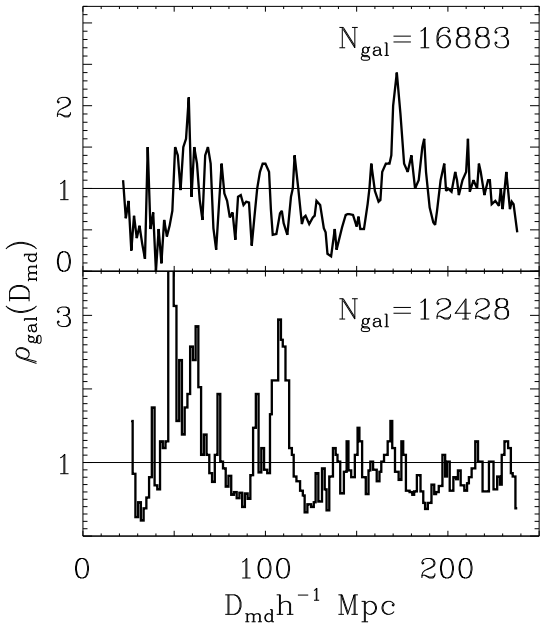

Figure 2. The normalized mean galaxy density in the modified samples N-600 (top panel) and S-600 (bottom panel).

The radial variations of the normalized number density of galaxies for both samples from Figure 1 are plotted in Figure 2. As is seen from this figure, the modified radial distances for the galaxies suppresses the very large-scale trends and emphasizes the smaller scale random variations in the density.

This correction is more important for the more distant regions of our samples ($D \geq 350h^{-1}$Mpc), which contain only ∼20% of galaxies. Thus, in the following analyses, we apply this correction only to the two deeper samples, the N-600 and the S-600. Of course, it cannot restore the lost information about the galaxy distribution in these regions, but it does help compensate the strong drop in the observed galaxy density at these distances and to apply the standard methods of investigation for the full catalogues with the depth $600h^{-1}$Mpc.

3 GENERAL CHARACTERISTICS OF OBSERVED LARGE SCALE STRUCTURE

To characterize the general properties of large scale spatial galaxy distribution we use the Minimal Spanning Tree (MST) technique applied to both directly observed samples of galaxies and to samples corrected for the selection effect. The MST technique was first discussed by Barrow, Bhavsar & Sonoda (1985) and by van de Weigaert (1991). Its applications for the quantitative description of observed and simulated catalogues of galaxies were discussed in Demiański et al. (2000) and Doroshkevich et al. (2000, 2001).

3.1 Wall-like and filamentary structure elements

With the MST technique we can demonstrate that the majority of galaxies is concentrated within wall-like structures and filaments which connect walls to joint random network of the cosmic web. The internal structure of both walls and filaments is complex. Thus, wall-like structures incorporate some fraction of filaments and both walls and filaments incorporate high density galaxy clouds. In particular, clusters of galaxies are usually situated within richer walls.

As is well known, for larger galaxy separations a Poisson-like point distribution can be expected for galaxies within structures. As a result, the probability distribution function of MST edge lengths (PDF MST), $W_{MST}(l)$, characterizes the geometry of the galaxy distribution. For the 1D and 2D Poissonian distributions typical for filaments and walls, respectively, $W_{MST}(l)$ is described by exponential and Rayleigh functions, namely,

$$W_{MST}(l) = \langle l \rangle^{-1} \exp(-l/\langle l \rangle)\,, \qquad (3)$$
$$W_{MST}(l) = 2l/\langle l^2 \rangle \exp(-l^2/\langle l^2 \rangle)\,.$$

Comparison of measured and expected PDFs MST allows us to demonstrate the existence of these two types of structure elements and to make approximate estimates of their richness.

In Fig. 3, we see plotted the $W_{MST}(l_{MST})$'s for the N-380 and S-380 samples. Note that these $W_{MST}(l_{MST})$'s are well fitted to a superposition of Rayleigh (at $l_{MST} \leq \langle l_{MST} \rangle$) and exponential (at $l_{MST} \geq \langle l_{MST} \rangle$) functions, thus confirming the high degree of galaxy concentration within the population of high density rich wall-like structures and less rich filaments.

3.2 High and low density regions

The methods for dividing a sample into subsamples of wall–like structures and filaments were proposed and tested in our previous publications (Demiański et al. 2000; Doroshkevich et al. 2000, 2001). The first step is to make a rough discrimi-

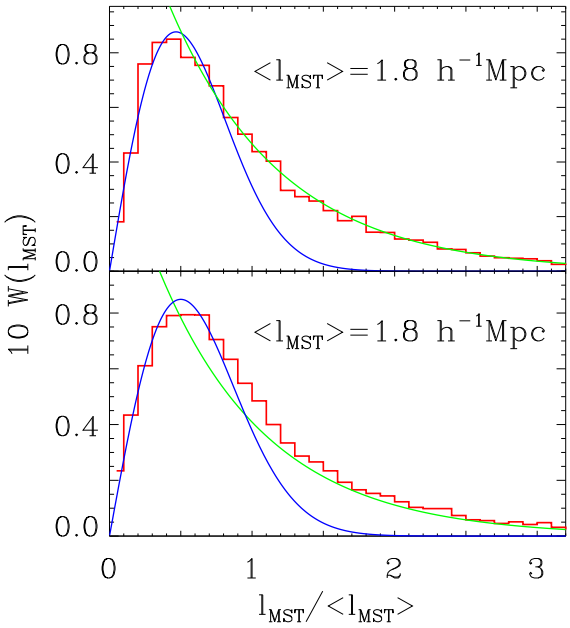

Figure 3. Distribution functions of MST edge lengths in redshift space for samples N-380 (top panel) and S-380 (bottom panel) are plotted by red lines. Rayleigh ($\approx 70\%$ of galaxies) and exponential fits are plotted by blue and green lines.

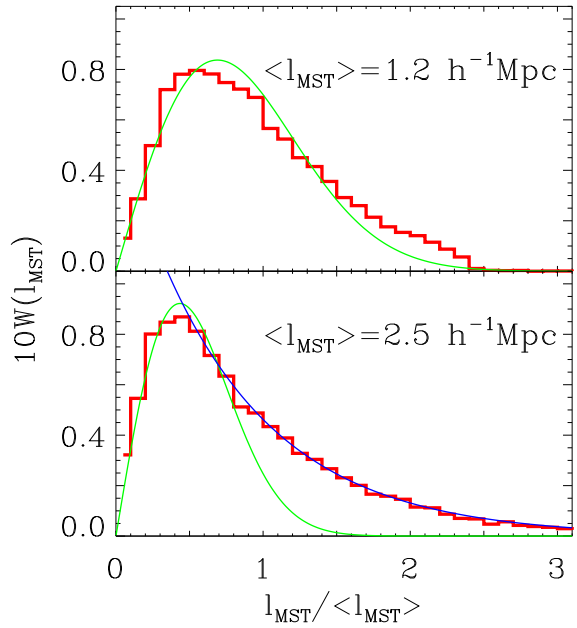

Figure 4. Distribution functions of MST edge lengths in redshift space for the HDRs (top panel) and LDRs (bottom panel). Rayleigh and exponential fits are plotted by green and blue lines.

nation between the high and low density regions (HDRs and LDRs).

Such discrimination can be easy performed for a given overdensity contour bounding the clusters and a given threshold richness of individual elements. In particular, to characterize the overdensity, δ_{thr}, we can use the threshold linking length, r_{lnk}, and a relation familiar from friends-of-friends algorithms (Huchra & Geller 1982):

$$\delta_{thr} = 3/[4\pi\langle n_{gal}\rangle r_{lnk}^3]\,. \tag{4}$$

In both the N-380 and S-380 samples, wall-like high density regions (HDRs) were identified with clusters found for a threshold richness $N_{thr} = 50$ and a threshold overdensity contour bounding the cluster equal to the mean density, $\delta_{thr} = 1$. For comparison, other samples of HDRs were separated with the same $N_{thr} = 50$ but a smaller threshold overdensity contour of $\delta_{thr} = 0.75$. These samples of HDRs contain 45% and 51% of all galaxies, respectively. The samples of low density regions (LDRs), which are occupied by filaments and poor groups of galaxies, are complementary to the HDRs in that the LDRs are simply the leftovers from the original total samples after the HDRs have been removed.

In Figure 4, the $W_{MST}(l)$ plotted for the HDRs is very similar to a Rayleigh function, thus confirming the sheet-like nature of the observed galaxy distribution within the HDRs.

The $W_{MST}(l)$ plotted for the LDRs also fits well to a Rayleigh function – at least for small edge lengths – indicating that $\sim 60\%$ of LDR galaxies are concentrated within less massive elliptical and sheet-like clouds. The LDR $W_{MST}(l)$ for larger edge lengths, however, appears to be closer to an exponential function, indicating that the remaining $\sim 40\%$ of LDR galaxies and some part of clouds are in filamentary structures.

The mean edge lengths, $\langle l_{MST}\rangle$, found for HDRs and LDRs separately, differ by about a factor of two, indicating that the difference in the mean density of HDRs and LDRs is about an order of magnitude.

3.3 Morphology of the structure elements

With the MST technique we can extract from within HDRs and LDRs themselves subsamples of structure elements for various threshold overdensities. We can then suitably characterize the morphology of each structure element by comparing the sum all edge lengths within its full tree, L_{sum}, with the sum of all edge lengths within the tree's trunk, L_{tr}, which is the longest path that can be traced along the tree without re-tracing any steps:

$$\epsilon = L_{tr}/L_{sum}\,. \tag{5}$$

For filaments, we can expect that the lengths of the full tree and of the trunk are similar to each other, whereas for clouds and walls these lengths are certainly very different. This approach takes into account the internal structure of each element rather than the shape of the isodensity contour bounding it, and, in this respect, it is complementary to the Minkowski Functional technique (see, e.g., Schmalzing at al. 1999).

However, even this method cannot discriminate between the wall-like and elliptical clouds and those rich filaments having many long branches for which again $\epsilon \leq 1$. This means that both the PDF of this ratio, $W(\epsilon)$, and the corresponding mass function, $f_m(\epsilon)$, are continuous functions and the morphology of structure elements can be more suitably characterized by the degree of filamentarity and 'wall-ness'. This also means that we can only hope to distinguish statistical differences between the morphologies of structure elements in HDRs and the morphologies of structure elements in LDRs.

The selection of clusters within HDRs and LDRs

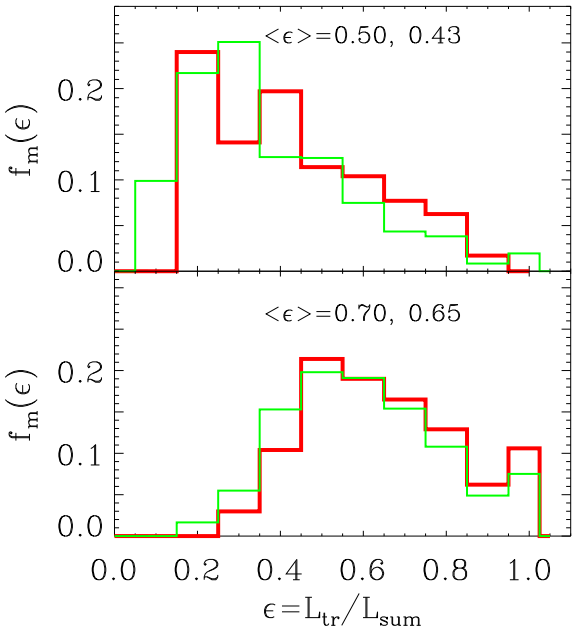

Figure 5. Mass functions of structure elements, $f_m(\epsilon)$, $\epsilon = L_{tr}/L_{sum}$ for the structure elements selected within HDRs with linking lengths $r_{link} = 2.$ & $2.4h^{-1}$Mpc (top panel, red and green lines) and within LDRs with linking lengths $r_{link} = 3.2$ & $3.6h^{-1}$Mpc (bottom panel, red and green lines).

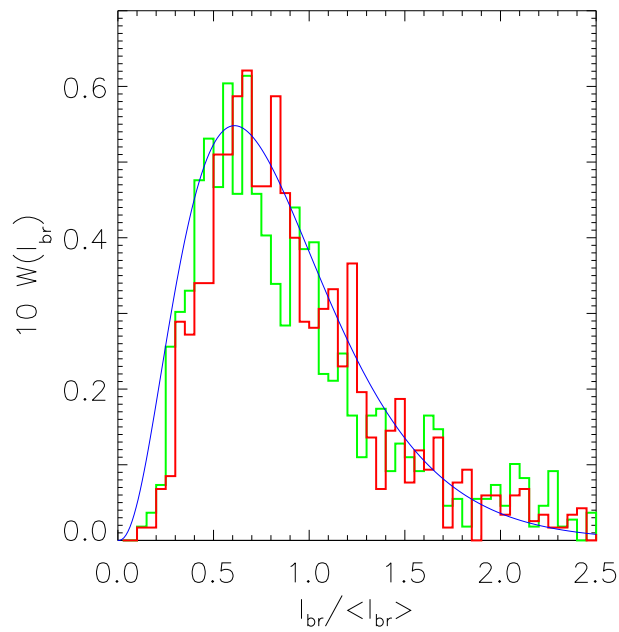

Figure 6. Distribution functions, W, for the distance between branch points along a trunk for filaments selected in LDRs with linking lengths $r_{lnk} = 3.2$ & $3.6h^{-1}$Mpc (red and green lines). Fit (6) is plotted by blue line.

was performed for two threshold linking lengths, $r_{lnk} = 2.$ & $2.4h^{-1}$Mpc for HDRs, and $r_{lnk} = 3.2$ & $3.6h^{-1}$Mpc for LDRs. The distribution functions of the ratio, $W(\epsilon)$, are found to be close to Gaussian with $\langle\epsilon\rangle \approx 0.5$ & 0.70 for HDRs and LDRs, respectively. The mass functions, $f_m(\epsilon)$, plotted in Fig. 5 for the same linking lengths, are shifted to left (for HDRs) and to right (for LDRs) in respect to the middle point.

These results verify the objective nature of the differences in the structure morphologies in HDRs and LDRs.

4 TYPICAL SIZE OF THE FILAMENTARY NETWORK

What is typical scale of the network of filaments spanning the LDRs? To estimate a measure of the cell size of the filamentary network, we extract filaments from the LDRs using clustering analysis like in Sec. 3.2. We then measure the distance between branch points along the trunk of these filamentary clusters. We take as the cell size of the filamentary network the mean distance between branch points averaged over all filaments. This definition of the filamentary network cell size differs from our definition in previous papers (e.g., Doroshkevich et al. 1996), where this cell size was defined as the mean free path between filaments. The present definition tends to yield cell sizes that are typically a factor of 1.5 – 2 smaller than those yielded by the mean-free-path definition.

Filaments can be extracted from the LDRs using different threshold overdensities (different linking lengths). However, filaments are connected to the network only for larger linking lengths; thus, the typical measured cell size depends upon the thresholds used. The distribution function of the separation of the branch points, $W(l_{br})$, is plotted in Fig. 6 for two linking lengths, $r_{lnk} = 3.2$ & $3.6h^{-1}$Mpc, which correspond to the threshold overdensities $\delta_{thr} = 0.66$ & 0.47. This distribution function is roughly fitted by expression

$$W(l_{br})dl_{br} \approx 42x^{2.5}\exp(-4.1x)\,dl_{br}, \quad x = l_{br}/\langle l_{br}\rangle\,, \qquad (6)$$

$$\langle l_{br}\rangle \approx 9.5 \;\&\; 11h^{-1}\mathrm{Mpc}\,.$$

These results are consistent with those obtained in Doroshkevich et al. (1996; 2001), where the mean free path between filaments for the Las Campanas Redshift Survey was found to be $\sim 12 - 17h^{-1}$Mpc.

5 PARAMETERS OF THE WALL–LIKE STRUCTURE ELEMENTS

The statistical characteristics of observed walls were first measured using the LCRS and DURS (Doroshkevich et al. 2000; 2001). The rich sample of walls extracted from the SDSS EDR, however, permits more refined estimates of the wall properties. As was discussed in Sec. 3.2 walls dominate the HDRs, and thus these subsamples of galaxies can be used to estimate the wall properties.

The expected characteristics of walls and methods of their measurement were discussed in Demiański et al. (2000); so here we will only briefly reproduce the main definitions. It is important that these characteristics can be measured independently in radial and transverse directions, which reveals the strong influence of the velocity dispersion on other wall characteristics.

Table 1. Wall properties in observed and simulated catalogues

sample	$\langle q_w\rangle/\Gamma$	$\tau_m/\sqrt{\Gamma}$	$\langle\delta_r\rangle$	$\langle\delta_t\rangle$	$\langle h_r\rangle$ h^{-1}Mpc	$\langle h_t\rangle$ h^{-1}Mpc	$\langle w_w\rangle$ km/s	$\langle D_{sep}\rangle$ h^{-1}Mpc
radial cores								
S-380	2.28 ± 0.58	0.58 ± 0.07	1.5	-	10.2 ± 1.6	-	293 ± 47	$53\pm\ 8$
S-600	2.26 ± 0.65	0.58 ± 0.08	1.4	-	10.5 ± 1.8	-	302 ± 52	58 ± 11
N-380	2.83 ± 0.73	0.65 ± 0.09	1.8	-	10.9 ± 1.4	-	316 ± 40	$70\pm\ 9$
N-600	2.57 ± 0.76	0.62 ± 0.09	1.3	-	13.5 ± 2.8	-	389 ± 81	74 ± 12
SDSS EDR	2.47 ± 0.72	0.61 ± 0.09	1.5	-	11.4 ± 2.5	-	329 ± 71	68 ± 13
transverse cores								
S-380	2.39 ± 0.78	0.60 ± 0.10	-	2.5	-	6.3 ± 1.3	-	57 ± 12
S-600	2.29 ± 0.64	0.58 ± 0.08	-	3.9	-	4.0 ± 0.8	-	58 ± 11
N-380	2.57 ± 0.74	0.62 ± 0.09	-	3.1	-	5.5 ± 1.0	-	77 ± 14
N-600	2.47 ± 0.51	0.61 ± 0.07	-	3.9	-	4.3 ± 0.8	-	65 ± 11
SDSS EDR	2.42 ± 0.67	0.60 ± 0.08	-	3.5	-	4.9 ± 1.3	-	64 ± 14
observed samples								
SDSS EDR	2.46 ± 0.7	0.60 ± 0.09	1.5	3.5	11.4 ± 2.5	4.9 ± 1.3	329 ± 71	66 ± 13
LCRS	2.51 ± 0.9	0.62 ± 0.10	3.0	7.4	8.6 ± 0.8	2.8 ± 0.7	247 ± 48	60 ± 10
DURS	2.23 ± 0.6	0.58 ± 0.08	1.7	6.5	9.7 ± 1.8	4.9 ± 1.2	280 ± 52	44 ± 10
mock catalogues in real and redshift spaces for the model with $\Gamma=0.2$								
redshift	2.7 ± 0.5	0.63 ± 0.06	1.8	3.8	11.8 ± 2.1	6.5 ± 1.4	338 ± 65	50 ± 10
real	2.1 ± 0.4	0.57 ± 0.06	4.3	4.6	4.8 ± 1.0	4.2 ± 1.0	305 ± 47	50 ± 10

5.1 Main wall characteristics

Main characteristic of walls is their mean dimensionless surface density, $\langle q_w\rangle$, measured by the number of galaxies per 1 Mpc^2 and normalized by the mean density of galaxies multiplied by a coherent length of initial velocity field (DD99; DD02)

$$l_v \approx 33h^{-1}\mathrm{Mpc}\ (0.2/\Gamma), \quad \Gamma=\Omega_m h\,, \tag{7}$$

where Ω_m is the mean matter density of the Universe. For Gaussian initial perturbations, the expected probability distribution function (PDF) of the surface density is

$$N_m(q_w)=\frac{1}{\sqrt{2\pi}}\frac{1}{\tau_m\sqrt{q_w}}\exp\left(-\frac{q_w}{8\tau_m^2}\right)\mathrm{erf}\left(\sqrt{\frac{q_w}{8\tau_m^2}}\right)\,, \tag{8}$$

$$\langle q_w\rangle = 8(0.5+1/\pi)\tau_m^2 \approx 6.55\tau_m^2\,.$$

This relation links the mean surface density of walls with the dimensionless amplitude of perturbations, τ_m,

$$\tau_m=\sqrt{\langle q_w\rangle/6.55}\,, \tag{9}$$

which can be compared with those measured by other methods (DD02).

Other important characteristics of walls are the mean velocity dispersion of galaxies within walls, $\langle w_w\rangle$, the mean separation between walls, $\langle D_{sep}\rangle$, the mean overdensity, $\langle\delta\rangle$, and the mean thickness of walls, $\langle h\rangle$. The mean velocity dispersion of galaxies, $\langle w_w\rangle$, can be measured in radial direction only whereas other wall characteristics can be measured both radially and along transverse arcs. Comparison of the wall thickness and the overdensity, $\langle h\rangle$ and $\langle\delta\rangle$, measured in transverse (t) and radial (r) directions, illustrates the influence of the velocity dispersion of galaxies on the observed wall thickness.

The velocity dispersion of galaxies within a wall w_w can be related to the radial thickness of the wall by this relation (Demiański et al. 2000):

$$h_r=\sqrt{12}H_0^{-1}w_w\,. \tag{10}$$

For a relaxed, gravitationally confined wall, the measured wall overdensity, surface density, and the velocity dispersion are linked by the condition of static equilibrium. Consider a wall as a slab in static equilibrium, and this slab has a nonhomogeneous matter distribution across it. We can then write the condition of static equilibrium as follows:

$$w_w^2=\frac{\pi G\mu^2}{\langle\rho\rangle\delta}\Theta_\Phi=\frac{3}{8}\frac{\Omega_m}{\delta}(H_0 l_v q_w)^2\Theta_\Phi\,, \tag{11}$$

Here $\mu=\langle\rho\rangle l_v q_w$ is the mass surface density of the wall and the factor $\Theta_\Phi\sim 1$ describes the nonhomogeneity of the matter distribution across the slab. Unfortunately, for these estimates we can only use the velocity dispersion and overdensity measured for radial and transverse directions, respectively, and, so, the final result cannot be averaged over the samples of walls.

5.2 Measurement of the wall characteristics

The characteristics of the walls can be measured with the two parameter core–sampling approach (Doroshkevich et al. 1996) applied to the subsample of galaxies selected within HDRs. With this method, all galaxies of the sample are distributed within a set of radial cores with a given angular size, θ_c, or within a set of cylindrical cores oriented along arcs of right ascension with a size d_c. All galaxies are projected on the core axis and collected to a set of one-dimensional clusters with a linking length, l_{link}. The one-dimensional clusters with richnesses greater than some threshold richness, N_{min}, are then used as the required sample of walls within a sampling core.

Both the random intersection of core and walls and the nonhomogeneous galaxy distribution within walls lead to

significant random scatter of measured wall characteristics. The influence of these factors cannot be eliminated, but it can be minimized for an optimal range of parameters θ_c, d_c, l_{link} and N_{min}. Results discussed below are averaged over the optimal range of these parameters.

Ten samples of HDR galaxies were used for the measurement of wall characteristics. Four of these HDR samples we saw in Sec. 3: the $\delta_{thr} = 1$ & $\delta_{thr} = 0.75$ samples for N-380 and for S-380. The other six HDR samples were extracted from the N-600 and S-600 catalogs corrected for radial selection effects (Sec. 2.1); the three different sets of threshold parameters employed yielded HDRs containing $\sim 42\%$, 44%, and 50% of all galaxies in the N-600 and S-600 catalogs.

For the radial measurements, the mean wall properties were averaged over three radial core sizes ($\theta_c = 2^\circ, 2.25^\circ$ and 2.5°) and for six core-sampling linking lengths ($2h^{-1}$Mpc$\leq l_{link} \leq 4.5h^{-1}$Mpc). For the transverse measurements, the mean wall properties were averaged over four core diameters ($d_c = 6.0$, 6.5, 7.0, and $7.5h^{-1}$Mpc) and five core-sampling linking lengths ($2h^{-1}$Mpc$\leq l_{link} \leq 4.h^{-1}$Mpc).

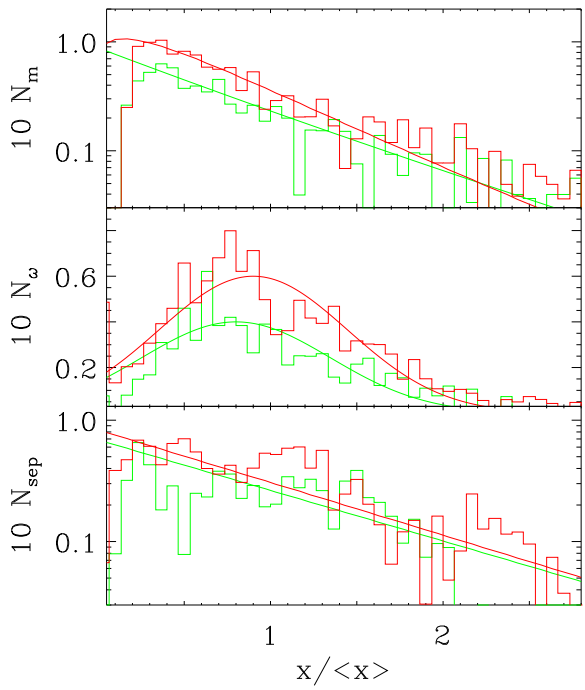

Figure 7. The PDFs of observed dimensionless surface density of walls, $N_m(q_w/\langle q_w\rangle)$ (8), reduced velocity dispersions within walls, $N_\omega(\omega_w/\langle\omega_w\rangle)$ (13), and wall separations, $N_{sep}(D_{sep}/\langle D_{sep}\rangle)$, averaged over radial samples of walls selected from samples S-380 (green lines) and N-380 (red line). Fits (8) for N_m, Gaussian fits for N_ω and exponential fits for N_{sep} are plotted by solid lines.

5.3 Measured characteristics of walls

The mean radial and tranverse wall properties for the N-380, S-380, N-600 & S-600 catalogs are listed separately in Table 1. Characteristics obtained by averaging over all ten samples are compared with those from the DURS and LCRS and with those from mock catalogues simulating the SDSS EDR (Cole 1998). The difference between the mean walls surface densities measured for samples N-380 and S-380 – $\sim$ 15– 20% – reflects real variations in the wall properties and an insufficient representativity of the two samples (i.e., cosmic variance). However, the scatters of mean values listed in Table 1 partially include the dispersions depending on the shape of their distribution functions. The actual scatter of mean characteristics of walls averaged over eight samples listed in Table 1 is also $\leq 10 - 12\%$.

The amplitude of initial perturbations characterized by values τ_m is similar for all eight listed SDSS EDR measurements and for the LCRS and the DURS. It is quite consistent with estimates found for simulations of the spatially flat ΛCDM cosmological model. The measured PDF of the surface density of walls plotted in Fig. 7 is well fitted to the expected expression (8). These results verify that, indeed, the observed walls represent recently formed Zel'dovich pancakes.

The difference between the wall thickness measured in the radial and transverse directions, h_r and h_t, indicates that, along a short axis, the walls are gravitationally confined stationary objects. Just as with the 'Finger of God' effect for clusters of galaxies, this difference characterizes the gravitational potential of compressed DM rather than the actual wall thickness. The same effect is seen as a difference between the wall overdensities measured in radial and transverse directions.

The difference between the wall thicknesses is compared with the velocity dispersions of galaxies within the walls, $\langle w_w\rangle$. Clusters of galaxies with large velocity dispersions incorporated in walls also increase the measured velocity dispersion. The correlation between the wall surface density and the velocity dispersion confirms the relaxation of matter within walls. This relaxation is probably accelerated due to strong small scale clustering of matter within walls.

Using measured mean wall characteristics we have for the parameter Θ_Φ introduced in equation (11)

$$\Theta_\Phi \approx \frac{\langle\delta\rangle}{3}\frac{0.3}{\Omega_m} \approx 1\,, \tag{12}$$

which is also quite consistent with the expected value for relaxed and stationary walls.

As was proposed in Demiański et al. (2000) we can discriminate between systematic variations in the measured velocity dispersion due to regular variations in the surface density along the walls (Fig. 7, top plot) and the random variations in the velocity dispersion due to, for instance, random intersections of a core with rich clusters embedded in a wall. Demiański et al. (2000) suggest for consideration a reduced velocity dispersion, ω_w,

$$\omega_w = w_w q_w^{-p_w}\,, \quad p_w \approx 0.5\,. \tag{13}$$

For this reduced velocity dispersion, ω_w, the systematic variations of w_w are suppressed and the Gaussian PDF, N_ω, can be expected. Indeed, this PDF plotted in Fig. 7 is similar to a Gaussian function.

Note that, for all the samples listed in Table 1, the mean wall separation, $\langle D_{sep}\rangle$, is close to twice of the coherent length of the initial velocity field,

$$\langle D_{sep}\rangle \approx 2l_v\,, \tag{14}$$

for the low density cosmological models with $\Gamma \approx 0.2$ (7). This results coincides with the estimates of the matter fraction – $\sim$ 50% – accumulated within walls. Due to the large

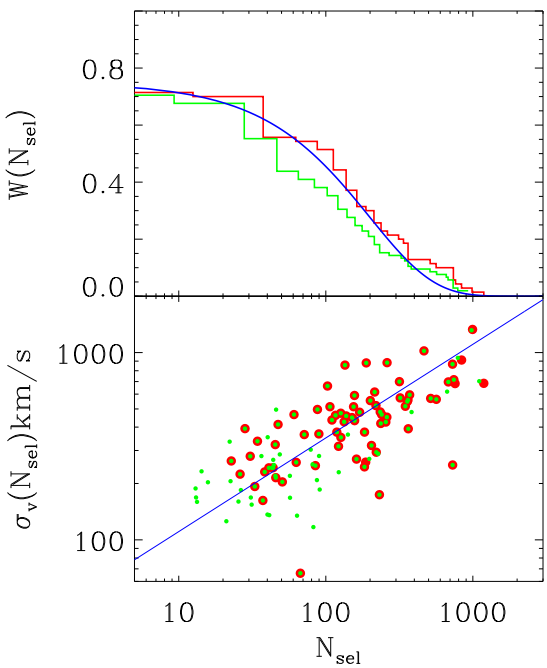

Figure 8. The distribution functions, $W(N_{sel})$ (top panel), and velocity dispersions within possible clusters of galaxies, $\sigma_v(N_{sel})$ (bottom panel), are plotted vs. the number of galaxies corrected for the selection effect, N_{sel}, for two samples of clusters with $N_{mem} \geq 10$ (green lines and points) and with $N_{mem} \geq 15$ (red lines and points). Fits (16) & (15) are plotted by blue lines.

separation of walls, the correlations of their positions is small and a random 1D Poissonian PDF of the separation can be expected. These PDFs are plotted in Fig. 6 together with the exponential fits.

Finally, we would like to draw attention to the fact that all measured properties of these walls are quite consistent with a CDM–like initial power spectrum and Gaussian distribution of perturbations.

6 POSSIBLE RICH CLUSTERS OF GALAXIES

The SDSS EDR also contains a number of massive galaxy clusters of various richnesses which can be extracted by means of the MST technique. Due to the large velocity dispersion of galaxies within clusters and the strong 'Finger of God' effect, this extraction must be performed using different threshold linking lengths in the radial (r_r) and in the transverse (r_t) directions. This is not unlike how group catalogs are extracted from redshift surveys using conventional 'friends-of-friends' algorithms (Huchra & Geller 1982; Tucker et al. 2000).

We performed this cluster-finding in two major steps. First, we projected the N-600 and the S-600 samples onto a sphere of radius $R = 100h^{-1}$ and extracted a set of candidate clusters from this 2D galaxy catalog using a transverse linking length of $r_t = 0.22h^{-1}$Mpc ($\delta_{th} \approx \mathbf{1}$). Second, we applied a radial linking length of $r_r = 4.5h^{-1}$Mpc to these candidate clusters using their (non-projected) 3D coordinates corrected for radial selection effects (eq. 2). In this second step, we also employed two threshold richness, $N_{mem} = 10$ & 15, for our final samples of possible rich clusters. Having extracted these probable rich clusters, we calculated a distance-independent measure of their richnesses by correcting their observed richnesses N_{mem} for radial selection effects using equation (1); we call this corrected richness N_{sel}. Let us remind that these are *possible* rich clusters of galaxies selected with the same algoritm; to confirm that they are physical potential wells, it would be best to check for diffuse x-ray emission.

For the threshold richness $N_{mem} = 10$, 70 and 37 possible rich clusters with $\langle N_{sel} \rangle = 186$ were selected from the N-600 and S-600 samples, respectively. For the larger threshold richness, $N_{mem} = 15$, 47 and 25 possible rich clusters with $\langle N_{sel} \rangle = 250$ were selected from the same samples. The majority of these clusters are embedded within richer walls. Note the significant excess of possible rich clusters in the north compared with the south – at least for distances $D \leq 600h^{-1}$Mpc.

For these possible clusters, sizes in the radial and transverse directions differ by factors of about 40 – 100, thus illustrating the 'Finger of God' effect. However, this ratio is determined in some part by the ratio of the chosen values of the radial and transverse linking lengths, r_r and r_t.

As is seen from Fig. 8, the richness of these possible clusters is strongly correlated with the radial size and velocity dispersion, σ_v,

$$\sigma_v \propto N_{sel}^{0.5} \,, \tag{15}$$

which is quite typical for relaxed gravitationally confined objects. For both the $N_{mem} \geq 10$ and the $N_{mem} \geq 15$ cluster samples, the distribution functions, $W(N_{sel})$, plotted in Fig. 8 are well fitted by the exponential function

$$W(N_{sel}) \propto \exp(-N_{sel}/200) \,. \tag{16}$$

7 MASS FUNCTION OF THE STRUCTURE ELEMENTS

The richness of the SDSS EDR allows one to extract several different sets of high density clouds and structure elements with various threshold overdensities within the HDRs and LDRs and to find their mass function. These results can be directly compared with the theoretical expectations of DD02.

Two samples of high density galaxy groups and two samples of unrelaxed structure elements – walls and filaments – were selected separately within HDRs and within LDRs for a threshold richness $N_{mem} \geq 5$. Since the velocity dispersions are expected to be much smaller than those in rich clusters, we select these samples of structure elements using the simpler method described in Sec. 4 rather than the two-step approach described in Sec. 6. The richness of each cluster was corrected for radial selection effects using the selection function introduced in Sec. 2.1.

The mass functions for these samples are plotted in Figure 9. The main properties of the selected clouds are listed in Table 2, where r_{lnk} and δ_{thr} are, respectively, the threshold linking length and corresponding threshold overdensity, f_{gal} is the fraction of galaxies from the total (combined HDR+LDR) sample of galaxies within the selected clouds, N_{cl} is the number of clouds, and $\langle N_{sel} \rangle$ is the mean richness of individual clouds corrected for the selection effect.

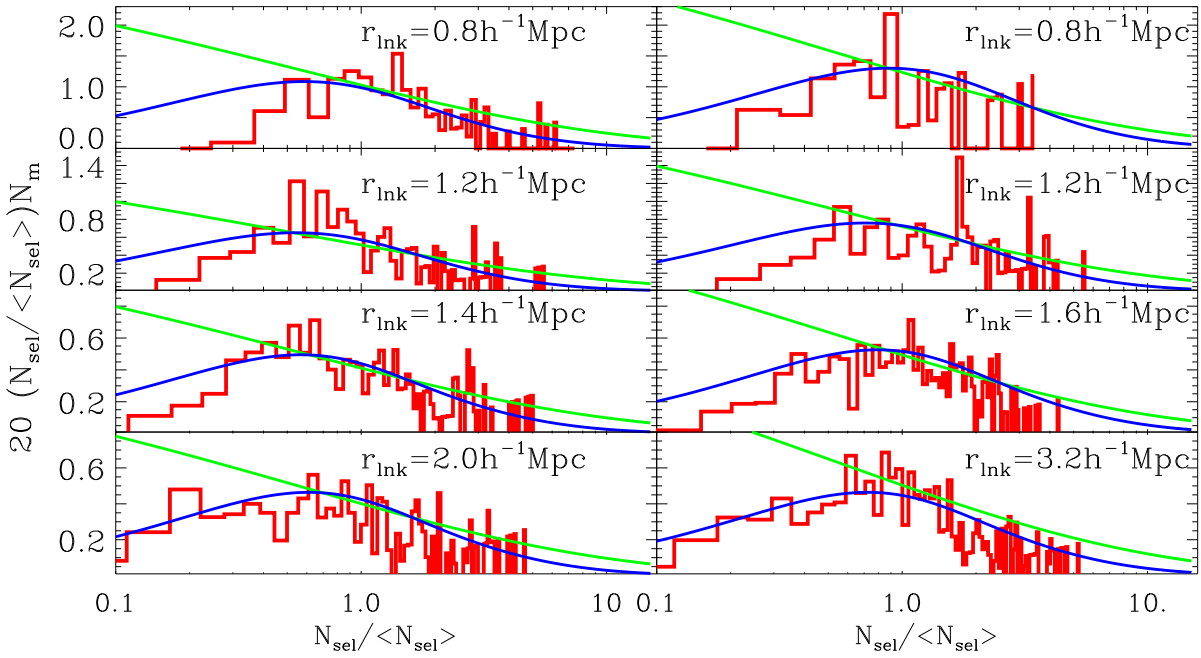

Figure 9. Mass functions galaxy clouds, $N(N_{sel}/\langle N_{sel}\rangle)$, selected in HDRs (left panels) and LDRs (right panels) for four threshold linking lengths. Fits for relaxed structures (eq. 17; $r_{lnk} = 0.8\&1.2h^{-1}$ Mpc) and for unrelaxed structures (eq. 18; $r_{lnk} = 1.4, 1.6, 2.0, \&3.2h^{-1}$ Mpc) are plotted by blue lines. Press-Schechter fits (eq. 19) are plotted by green lines.

As was shown in DD02, in Zel'dovich theory and for the WDM initial power spectrum the dark matter mass function of structure elements is independent of their shapes and, at small redshifts, it can be approximated by the functions

$$xN(x)dx = 12.5\kappa_{ZA}x^{2/3}\exp(-3.7x^{1/3})\ \mathrm{erf}(x^{2/3})dx\,, \qquad (17)$$

$$xN(x)dx = 8.\kappa_{ZA}x^{1/2}\exp(-3.1x^{1/3})\ \mathrm{erf}(x^{3/4})dx\,. \qquad (18)$$

$$x = \mu_{ZA}\frac{M}{\langle M\rangle}\,,$$

The expression (17) relates to clouds which have become essentially relaxed and static by $z = 0$, and the expression (18) relates to richer, unrelaxed filaments and walls which are still in the process of collapse. Here, $\kappa_{ZA} \sim 1.5 - 4$ and $\mu_{ZA} \sim 0.8 - 1.3$ are fit parameters which take into account the incompleteness of selected samples of clouds for small and large richnesses; this incompleteness changes both the amplitude and mean mass of the measured clouds. Comparison with simulations (DD02) has shown that these relations fit reasonably well to the mass distribution of structure elements.

For comparison, we can use the mass function from the Press-Schechter formalism,

$$xN_{PS}(x)dx = \frac{8\kappa_{PS}}{45\sqrt{\pi}}\ \xi^{1/6}\exp(-\xi^{1/3})dx\,, \qquad (19)$$

$$\xi = 1.785\mu_{ps}x = 1.785\mu_{ps}M/\langle M\rangle\,.$$

Here again the fitting parameters κ_{PS} and μ_{PS} take into account the incompleteness of measured sample. This expression relates to the CDM-like power spectrum without small scale cutoff linked, for example, with the finite mass of DM particles, and without correction for the survival probability. So, it does not describe the less massive part of the mass function.

Table 2. Parameters of groups of galaxies selected in HDRs and LDRs after correction for the selection effect.

$r_{lnk}h^{-1}$Mpc	δ_{thr}	f_{gal}	N_{cl}	$\langle N_{sel}\rangle$
		HDR		
0.8	45.	0.08	222	16.4
1.2	13.4	0.2	403	34.2
1.4	8.3	0.25	416	44.4
2.0	2.9	0.4	725	90.
		LDR		
0.8	45.	0.02	58	18.8
1.2	13.4	0.06	197	22.7
1.6	5.6	0.13	396	39.6
3.2	0.8	0.34	1176	84.8

Relations (17), (18), & (19) characterize the mass distribution of dark matter clouds associated with the observed galaxy groups and massive structure elements. They are closely linked with the initial power spectrum and quite similar to each other despite the fact that they use different assumptions about the process of cloud formation and the shape of the formed clouds. Both the Zel'dovich and Press-Schechter formalisms plotted in Fig. 9 fit reasonably well the observed mass distribution at $N_{sel} \geq \langle N_{sel}\rangle$, where the exponential term in (17), (18), & (19) dominates.

For $N_{sel} \leq \langle N_{sel}\rangle$ the incompleteness of the sample of selected clouds leads to the rapid drops in the observed mass functions as compared with theoretical expectations. However, for the largest linking lengths, $r_{lnk} = 2.0$ & $3.2h^{-1}$Mpc, where this incompleteness is minimal, the observed mass distribution is quite consistent with theoretical expectations.

For very large values of r_{lnk}, some excess of very massive clouds is generated due to the impact of the percolation

process, which results in the formation of the network of filaments and the largest walls. This process is not described by the theoretical expressions (17), (18) & (19).

Results listed in Table 2 illustrate the influence of environment on the properties of high density clouds. In particular, in spite of the approximately equal number of galaxies in HDRs and LDRs, the majority of the high density clouds selected with linking lengths $r_{lnk} = 0.8$ & $1.2h^{-1}$Mpc are situated within the HDRs.

8 SUMMARY AND DISCUSSION

Statistical analysis of large galaxy redshift surveys allows us to obtain the quantitative characteristics of large scale galaxy distribution, which in turn can be related to the fundamental characteristics of the Universe and the processes of structure formation. The large homogeneous data set compiled in the SDSS EDR also permits us to checking the results from analysis of the LCRS and the DURS and to obtain more accurate and more representative estimates of the main basic characteristics of the Universe.

The spatial galaxy distribution for the N-600 and S-600 samples is plotted in Figs. 10 & 11; galaxies in HDRs and in rich clusters are highlighted.

8.1 Main results

The main results of our investigation can be summarized as follows:

(i) The analysis performed in Sec. 3 with the MST technique confirms that about half of galaxies are situated within rich wall – like structures and the majority of the remaining galaxies are concentrated within filaments. This result confirms that the filaments and walls are the main structure elements in the observed galaxy distribution. Quantitative characteristics of walls and filaments presented in Sections 3, 4 & 5 validate this division of the LSS into these two subpopulations.

(ii) The typical cell size of the filamentary network is found to be $\sim 10h^{-1}$Mpc. This estimate is consistent with the one obtained previously for the LCRS (Doroshkevich et al. 1996, 2001).

(iii) The main characteristics of wall–like structure elements, such as the overdensity, separation distance between walls, wall thickness, and the velocity dispersion within walls, were measured separately for radial and transverse directions in the SDSS EDR equatorial stripes. Comparison of these characteristics demonstrates that the walls are in static equilibrium, that they are relaxed along their shorter axis, and that their thickness in radial direction is defined by the velocity dispersion of galaxies.

(iv) The PDF of the wall surface density is consistent with that predicted by Zel'dovich theory for Gaussian initial perturbations. The measured amplitude of perturbations coincides with that expected for a CDM-like initial power spectrum and spatially flat ΛCDM cosmological model with $\Omega_\Lambda \approx 0.7$ and $\Omega_m \approx 0.3$.

(v) The MST technique permits the extraction of rich galaxy clusters from the full observed sample of galaxies. It is found that the rich selected clusters are situated mainly within richer walls and that their richness correlates with the measured velocity dispersion of galaxies.

(vi) The mass distributions of groups of galaxies, filaments and walls selected with various threshold overdensities are quite well fitted to the joint mass function consistent with the expectations of Zel'dovich theory.

8.2 Northern and southern samples

The observations of both northern and southern samples were performed in the same manner; so comparison of these samples can characterize their statistical representativity.

As is seen from Figs. 1 – 3, the general properties of both samples are quite similar. Thus, for both samples the radial selection effects are described by a single function with the same selection scale, R_{sel}. Furthermore, the spatial galaxy distributions in both the N-380 and the S-380 samples are characterized by the same mean MST edge lengths, and the same fractions of galaxies can be assigned to the wall – like and filamentary components.

Nonetheless, the comparison of the wall properties listed in Table 1 already shows some differences – at the $\sim 10\%$ level – between the wall richnesses for the northern and southern samples. A stronger difference – by roughly a factor of 2 – is seen in the number of rich galaxy clusters extracted from these two samples. The same north-south difference is seen in the total number of galaxies incorporated into these clusters. Part of this factor-of-two difference, of course, is due to the different size areas covered by the northern and southern samples – the northern sample is about 1.4× larger than the southern. The remaining difference – a factor of $2.0/1.4 = 1.4$ – is likely due to cosmic variance.

This north-south comparison demonstrates that the achieved richness of samples under investigation is sufficient to characterize the general properties of the large scale spatial galaxy distribution, but it becomes insufficient for discussing the properties of the rarer walls and the rich clusters of galaxies.

8.3 Properties of walls

The walls and filaments are the largest structure elements observed in the Universe. In contrast to galaxies, their formation occurs at relatively small redshifts in course of the last stage of nonlinear matter clustering and is driven by the initial power spectrum of perturbations. Therefore, their properties can be successfully described by the nonlinear theory of gravitational instability (Zel'dovich 1970) that allows us to link them with the characteristics of initial power spectrum.

The interpretation of the walls as Zel'dovich pancakes has been discussed already in Thompson and Gregory (1978) and in Oort (1983). The comparison of the statistical characteristics of the Zel'dovich pancakes for a CDM–like initial power spectrum (DD99, DD02) with those for observed walls demonstrates that, indeed, this interpretation is correct and, for a given cosmological model, it allows us to obtain independent estimates of the fundamental characteristics of the initial power spectrum.

The estimates of the mean wall surface density, $\langle q_w \rangle$, and the amplitude of initial perturbations, $\langle \tau_m \rangle$, listed in

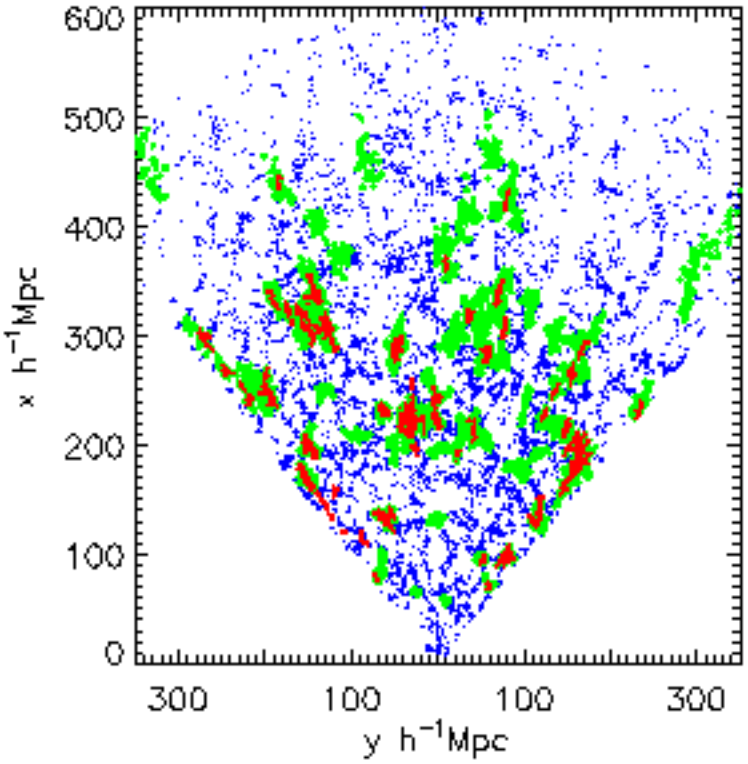

Figure 1. Spatial distribution of all galaxies in the sample N-600 (blue points), galaxies within the HDRs (green points), and within possible rich clusters of galaxies (red points).

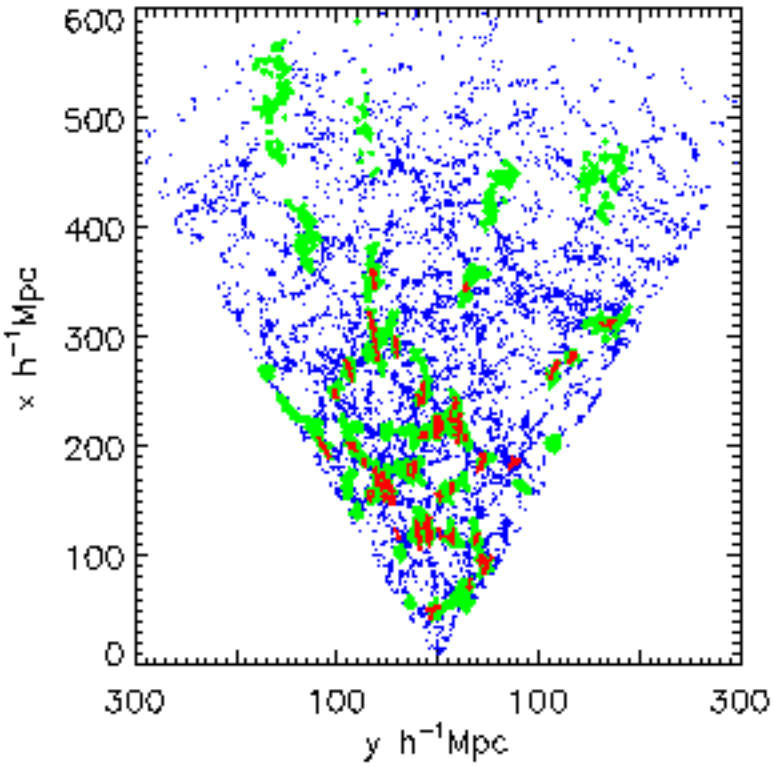

Figure 2. Spatial distribution of all galaxies in the sample S-600 (blue points), galaxies within the HDRs (green points), and within possible rich clusters of galaxies (red points).

Table 1 for eight samples of walls are consistent with each other and with those found for the LCRS and DURS. They are also close to those found for the simulated DM distribution and for the mock galaxy catalogs (Cole et al. 1998) prepared for a spatially flat ΛCDM cosmological model with $\Omega_\Lambda = 0.7$ and $\Omega_m = 0.3$.

The scatter in $\langle q_w \rangle$ and $\langle \tau_m \rangle$ listed in Table 1 includes partly the dispersions generated by the shape of the distribution function of q_w for a single measurement. Averaging of both $\langle q_w \rangle$ and $\langle \tau_m \rangle$ listed in Table 1 for eight samples of walls allows us to estimate the scatter in the mean values as follows:

$$\langle q_w \rangle = (0.49 \pm 0.03)(\Gamma/0.2)\,, \tag{20}$$

$$\tau_m = (0.27 \pm 0.028)\sqrt{\Gamma/0.2}\,, \tag{21}$$

thus characterizing the variations in the mean wall properties for the samples under investigation.

The amplitude of initial perturbations (eq. 21) is consistent with estimates τ_{CMB} (DD99; DD02)

$$\tau_{CMB} \approx 0.27\sqrt{\Gamma/0.2} \tag{22}$$

obtained from the measurements of angular variations of CMB temperature (Bunn & White 1997) for the same spatially flat ΛCDM cosmological model. The measured PDF of the surface density of walls plotted in Fig. 6 is well fitted to the expression (8) expected for the Gaussian initial perturbations (DD99; DD02).

These results verify that, indeed, the observed walls are recently formed Zel'dovich pancakes. They verify also the Gaussian distribution of initial perturbations and coincide with the Harrison – Zel'dovich primordial power spectrum.

Comparison of other wall characteristics measured in radial and transverse directions indicates that the walls are gravitationally confined and relaxed along the shorter axis. The same comparison allows us to find the true wall overdensity, wall thickness, and the radial velocity dispersion of galaxies within walls. As is seen from relation (11), these values are quite self–consistent.

8.4 Possible rich clusters of galaxies

Samples of possible rich clusters of galaxies extracted from the N-600 and S-600 samples demonstrate mainly the technical abilities of the MST code. The physical reality of these clusters would be best tested, however, with independent x-ray observations.

Nonetheless, some characteristics of these clusters seem to be reasonably consistent with expectations. Thus, as is seen from Figs. 10 & 11, these clusters are situated mainly within the richer walls, their richness and velocity dispersion are linked by relation (15), and their mass function plotted in Fig. 8 is similar to an exponential and is dissimilar to the mass functions seen for groups of galaxies and unrelaxed structure elements discussed in Sec. 7 . Large differences between the number of clusters in the N-600 and S-600 samples demonstrate an insufficiently representative volume for these relatively rare structures (remember that rich clusters typically only contain about 10% of all galaxies).

8.5 Mass function of structure elements

Rich samples of walls, filaments, and groups of galaxies in the SDSS EDR selected using different threshold overdensities allow us to measure their mass functions, to trace their dependence on the threshold overdensity, and to compare them with the expectations of Zel'dovich theory.

This comparison verifies that, for lower threshold overdensities for both filaments and wall–like structure elements, the shape of the observed mass functions is consistent with the expectations of Zel'dovich theory. For groups of galaxies, however, a deficit of low mass groups caused presumably by selection effects and enhanced by the restrictions inherent in our procedure for group-finding leads to a stronger difference between the observed and expected mass functions for $N_{sel} \leq \langle N_{sel} \rangle$.

Let us note, that both mass functions, (17, 18, & 19), are closely linked with the initial power spectrum. They differ from the mass function of galaxy clusters, (16), and the probable mass function of observed galaxies which are formed on account of multy step merging of less massive clouds and are described by the power law with an exponential cutoff (see, e.g., Silk & White (1978).

8.6 Final comments

The SDSS (York et al. 2000) and 2dF (Colless et al. 2001) galaxy redshift surveys provide deep and broad vistas with which cosmologists may study the galaxy distribution on extremely large scales – scales on which the imprint from primordial fluctuation spectrum has not been erased.

In this paper, we have used the SDSS EDR to investigate these large scales. We have confirmed our earlier results, based on the LCRS and DURS samples, that galaxies are distributed in roughly equal numbers between two different environments: filaments, which dominate low density regions, and walls, which dominate high density regions. Although different in character, these two environments together form a broken joint random network of galaxies – the cosmic web.

Comparison with theory strongly supports the idea that the properties of the observed walls are consistent with those for Zel'dovich pancakes formed from a Gaussian spectrum of initial perturbations for a flat ΛCDM Universe ($\Omega_\Lambda \approx 0.7$, $\Omega_m \approx 0.3$). These results are well consistent to the estimate $\Gamma = 0.20 \pm 0.03$ obtained in Percival et al. (2001) for the 2dF Galaxy Redshift Survey.

These are important, basic conclusions regarding the large scale structure of the Universe. With future public releases of the SDSS data set, we hope to refine these conclusions.

ACKNOWLEDGMENTS

We thank Shiyin Shen of the Max-Planck-Institut für Astrophysik and Jörg Retzlaff of the Max-Planck-Institut für Extraterrestrial Physics for useful discussions regarding this work.

Funding for the creation and distribution of the SDSS Archive has been provided by the Alfred P. Sloan Foundation, the Participating Institutions, the National Aeronau-

tics and Space Administration, the National Science Foundation, the US Department of Energy, the Japanese Monbukagakusho, and the Max Planck Society. The SDSS Web site is http://www.sdss.org/.
The Participating Institutions are the University of Chicago, Fermilab, the Institute for Advanced Study, the Japan Participation Group, the Johns Hopkins University, the Max Planck Institute for Astronomy (MPIA), the Max Planck Institute for Astrophysics (MPA), New Mexico State University, Princeton University, the United States Naval Observatory, and the University of Washington.
This paper was supported in part by Denmark's Grundforskningsfond through its support for an establishment of the Theoretical Astrophysics Center.

REFERENCES

Barrow J., Bhavsar S., Sonoda D., 1985, MNRAS, **216**, 17
Baugh C.M., & Efstathiou G., 1993, MNRAS., 265, 145.
Cole S., Hatton, S., Weinberg D.H. & Frenk C.S., 1998, MNRAS, 300, 945.
Colless M., et al., 2001, MNRAS, 328, 1039
Demiański M. & Doroshkevich A., 1999, MNRAS, 306, 779 (DD99)
Demiański M., Doroshkevich A., Müller V., & Turchaninov V.I., 2000, MNRAS., 318, 1177,
Demiański M. & Doroshkevich A., 2002, MNRAS, submitted (DD02)
Doroshkevich A., et al., 1996, MNRAS, 284, 1281,
Doroshkevich A., et al., 2000 MNRAS, 315, 767
Doroshkevich A., et al., 2001, MNRAS, 322, 369
Doroshkevich A., Allam S., Tucker D., in preparation
Fukugita M., Ickikawa T., Gunn J.E., Doi M., Shimasaku K., Schneider D.P., 1996, AJ, 111, 1748
Gunn J.E. et at., 1998, AJ, 116, 3040
Huchra J.P., Geller M.J., 1982, ApJ, 257, 423
Jenkins A. et al., 1998, ApJ., 499, 20.
Oort J.H., 1983a, Ann.Rev.Astron.Astrophys., 21, 373
Percival W.J. et al., 2001, MNRAS, 327, 1297
Ratcliffe A. et al., 1996, MNRAS 281, L47
Schmalzing J., Gottlöber S., Klypin A., Kravtsov A., 1999, MNRAS, 309, 1007.
Shandarin S., Zel'dovich Ya.B., 1989, Rev.Mod.Phys., 61, 185
Shectman S.A. et al., 1996, ApJ, 470, 172
Silk J. and White S.D.M., 1978, ApJ., 223, L59
Stoughton S. et al. 2002, AJ, 123, 485; 576
Thompson L.A., Gregory S.A., 1978, ApJ. 220, 809.
Tucker D.L. et al., 2000, ApJS, 130, 237.
van de Weygaert R., 1991, Ph.D. Thesis, University of Leiden
York D.G. et al. 2000, AJ, 120, 1579
Zel'dovich Ya.B., 1970, A&A, 5, 20

APPENDIX

As mentioned in Sec. 2, we obtained our SDSS EDR sample via the SDSS Query Tool (`sdssQT`), a standalone interface to the SDSS Catalog Archive Server. We performed the following query to obtain our particular sample of SDSS galaxies:

```
SELECT
tag.photoobj.field.segment.run,
tag.photoobj.field.segment.rerun,
tag.photoobj.field.segment.camCol,
tag.photoobj.field.field,
tag.photoobj.objid,
tag.photoobj.ra,
tag.photoobj.dec,
tag.g,
tag.g-tag.r,
z,zErr,
(primTarget & 32)+(primTarget & 67108864)
FROM
SpecObj
WHERE
zConf > 0.95
&&
specClass == 2
&& ( (primTarget & 64) > 0 ||
(primTarget & 128) > 0 ||
(primTarget & 256) > 0 )
```

This query chooses objects which were targetted as part of the main galaxy sample –

```
(primTarget & 64) > 0 ||
(primTarget & 128) > 0 ||
(primTarget & 256) > 0
```

and were found to have galaxy spectra –

```
specClass == 2
```

As an added bonus, this query notes which of these objects targetted as part of the main galaxy sample are also classified as luminous red galaxies (LRGs; Eisenstein et al. 2002):

```
(primTarget & 32)+(primTarget & 67108864)
```

These LRGs and their place in the general distribution of galaxies will be discussed in a future paper (Doroshkevich, Allam, & Tucker 2003).